2011 50th IEEE Conference on Decision and Control and
European Control Conference (CDC-ECC)
Orlando, FL, USA, December 12-15, 2011

Maximum Power Point Tracking for Photovoltaic Systems Using Adaptive Extremum Seeking Control

Xiao Li, Yaoyu Li, *Member, IEEE*, John E. Seem, *Member, IEEE* and Peng Lei

Abstract — **To maintain the maximum achievable efficiency for the photovoltaic (PV) systems, it is crucial to achieve the maximum power point tracking (MPPT) operation for realistic illumination conditions. This paper presents the application of the adaptive extremum seeking control (AESC) scheme to the PV MPPT problem. A state-space model is derived for the PV system with buck converter. The AESC is used to maximize the power output by tuning the duty ratio of the pulse-width modulator (PWM) of the DC-DC buck converter. To address the nonlinear PV characteristics, the radial basis function (RBF) neural network is used to approximate the unknown nonlinear *I-V* curve. The convergence of the system to an adjustable neighborhood of the optimum is guaranteed by utilizing a Lyapunov-based adaptive control method. The performance of the controller is verified through simulations.**

I. Introduction

SOLAR power has experienced dramatic growth in the past decade, and the Solar Energy Industries Association (SEIA) predicts that the global capacity will reach 980 GW by 2020 [1]. A photovoltaic solar power system directly converts solar irradiation into electricity [2] [3]. In order to reduce the cost of energy (COE), it is ideal to maintain the PV operation at its maximum efficiency any time, and such goal is complicated by uncertain nonlinear current-voltage (*I-V*) and power-voltage (*P-V*) characteristics due to the changes in intrinsic and environment conditions [4]. The so-called Maximum Power Point tracking (MPPT) is a crucial aspect of control design for PV system operation [2].

Many MPPT techniques have been proposed [2, 5-8], and most of them utilize the feedback of power measurement of the PV array. Typical MPPT methods are essentially static search, such as the perturbation and observation (P&O) method [6], the incremental conductance (IncCond) method [9] and the hill climbing (HC) method [10]. Such methods may be limited when the system undergoes quick change of the environment conditions. More dynamic MPPT control methods [11-13] have been investigated. The dither-demodulation type of Extremum Seeking Control (ESC) strategy has received a lot of attention, as capable of nearly model-free search of the optimal input [14, 15]. The dither ESC based MPPT methods have been investigated in the past several years [7, 16]. Lei et al. [7, 16] have demonstrated the application of such ESC for the PV MPPT, which can simultaneously detects the change in internal resistance from the dithered transient. However, the drawback of such ESC scheme is its validity limited to the neighborhood of the optimum (equilibrium) point, and the controller design is based on certain assumed functions e.g. quadratic. Variation in the actual nonlinear mapping cannot be taken into account explicitly, which may limit its performance. The PV power-voltage characteristic (Fig. 2b) presents a good example of such situation. The curve bears very different slopes at both sides of the MPP. As a safe choice, the ESC loop gain has to be limited by the steeper side, which may lead to slow convergence if searching from the low-voltage side.

Such problem is approached from a different perspective in this study, by following the *Adaptive Extremum Seeking Control (AESC)* recently developed by Guay and his co-workers [17-19]. The AESC controller is designed based on the knowledge of system model structure and certain objective function [20]. A parameter learning law is used to approximate the unknown nonlinear relationship between states, and a Lyapunov based inverse optimal design technique is used to ensure the convergence to the optimum. Such ESC scheme searches for both the actual parameters and the optimal input simultaneously. As the asymmetry of the nonlinear map is dealt with by the parameter learning process, the AESC is expected to achieve better transient performance in the PV MPPT. In particular, the PV output power is simply the product of the terminal voltage and current, thus the objective function is hinged on the nonlinear characteristics of $I(V)$. The radial basis function (RBF) with Gaussian kernels [21] is used to approximate the unknown $I(V)$ characteristics. A Lyapunov-based adaptive learning control technique [22] is applied to guarantee the convergence of the overall system output to an adjustable, approximation error dependent neighborhood of the optimum.

The remainder of this paper is structured as follows. Section II presents the PV simulation model used, along with the DC-DC converter. The AESC design framework is briefly reviewed in Section III. In Section IV, the AESC and the parameter estimation algorithm are developed based on the approximated analytical modeling of PV dynamics following

Manuscript received March 22, 2011. This work was supported by the Johnson Controls, Inc.

Xiao Li is with University of Wisconsin - Milwaukee, 3200 N. Cramer St., Milwaukee, WI 53211, USA (corresponding author; tel: (414) 426-7497; e-mail: xiaoli@uwm.edu).

Yaoyu Li is with University of Texas at Dallas, 800 W. Campbell Rd., Richardson, TX 75080, USA (e-mail: yaoyu.li@utdallas.edu).

John E. Seem is with Building Efficiency Research Group, Johnson Controls, Inc., 507 E. Michigan St., Milwaukee, WI 53209, USA (e-mail: john.seem@gmail.com).

Peng Lei is with University of Wisconsin-Milwaukee, 3200 N. Cramer St., Milwaukee, WI 53211, USA (e-mail: penglei@uwm.edu)

the spirit of [22]. Simulation results are shown in Section V, with conclusion given in Section VI.

II. Photovoltaic System Model

The equivalent circuit of the PV system is shown in Fig. 1 [3], and its current-voltage relation can be modeled as [3]

$$I = I_{PV} - I_0\left[\exp\left(\frac{V+R_sI}{V_ta}\right)-1\right]-\frac{V+R_sI}{R_p} \tag{1}$$

where V and I are the output voltage and current, respectively, and I_0 is the reverse saturation (or leakage) current of the diode. $V_t = N_skT/q$ is the thermal voltage of the array with N_s cells connected in series, q = 1.60217646 $\times 10^{-19}$ C is the electron charge, and k = 1.3806503 $\times$ 10^{-23} J/K is the Boltzmann constant. N_p is the number of cells in parallel, a is the ideality factor, and R_s and R_p are the equivalent series and shunt resistance, respectively. I_{PV} is the photocurrent proportional to the irradiance, and is also influenced by the temperature [3]:

$$I_{PV} = \left(I_{PV,n} + K_I\Delta T\right)\frac{G}{G_n} \tag{2}$$

where $I_{PV,n}$ is the light generated current at the nominal condition (25°C and 1000W/m^2) , and $\Delta T = T - T_n$, with T and T_n being the actual and nominal temperatures, respectively. G and G_n are the actual and nominal irradiance rate on the device surface. K_I is the short-circuit temperature coefficient. The leakage current is [3]:

$$I_0 = I_{0,n}\left(\frac{T_n}{T}\right)^3\exp\left[\frac{qE_g}{ak}\left(\frac{1}{T_n}-\frac{1}{T}\right)\right] \tag{3}$$

where E_g is the bandgap energy of the semiconductor and $I_{0,n}$ is the nominal saturation current.

The simulation in this study adopts a PV array with 15×2 modules, and each module has 54 cells in series. R_P = 322Ω and R_S = 0.075Ω. Figure 2 shows the I-V and P-V characteristics at 25 °C under different irradiances, while Figure 3 shows the I-V and P-V characteristics under nominal irradiance rate 1000W/m^2 at different temperatures. The power output decreases with the increase of device temperature. Notice that the MPP voltage is also shifted for all cases in Figs. 2 and 3, while the temperature change leads to more pronounced changes. This indicates that the adaptive MPPT could be more beneficial for temperature change.

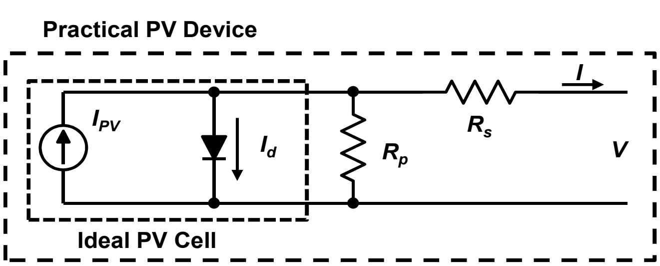

Fig. 1. PV Cell Equivalent Circuit.

As this study aims to validate an MPPT control algorithm, a simple scenario of DC resistive load is adopted, as shown in Fig. 4. The duty ratio D of the pulse-width modulator (PWM) is used to adjust the input voltage of the buck DC-DC converter to achieve MPPT.

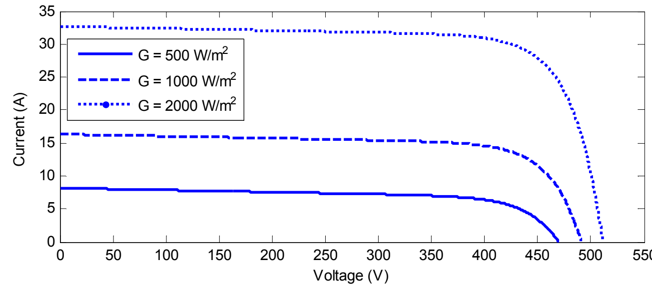

(a) I-V Curves

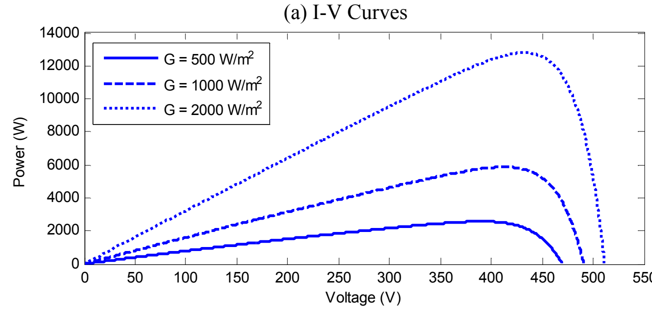

(b) P-V Curves

Fig. 2 I-V and P-V Curves at 25 °C under Different Irradiance Rates

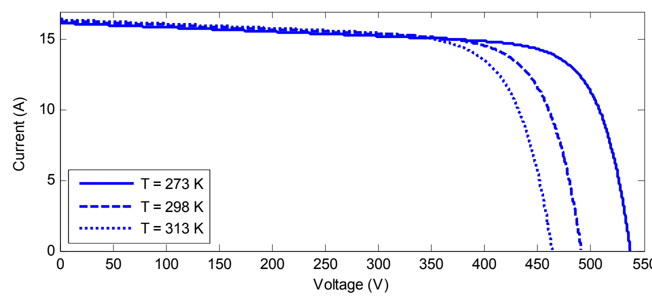

(a) I-V Curves

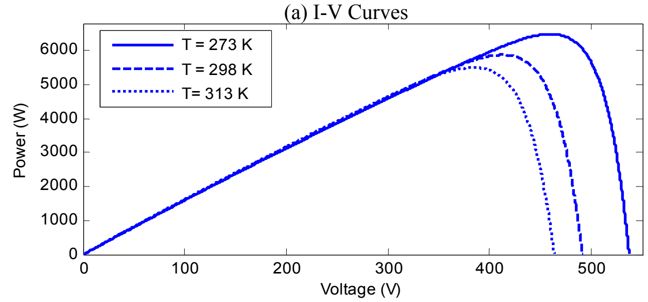

(b) P-V Curves

Fig. 3 I-V and P-V Curves at Irradiance Rate 1000W/m^2, under Different Temperatures

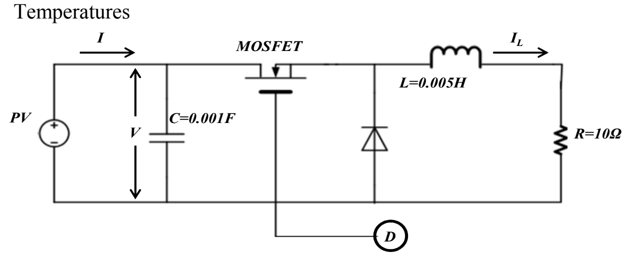

Fig. 4. PV Array with Front-end Buck Converter.

III. Review Of Adaptive Extremum Seeking Control

The adaptive extremum seeking control is to find the unknown operating set-points that optimize the desired objective function [20]. Consider the dynamic system form of

[22]:

$$\dot{x} = f\left[x, \mu(x), u\right] \quad (4)$$

$$y = h\left[x, \mu(x)\right] \quad (5)$$

where the objective function output y is assumed not to be directly measureable for feedback, the explicit structure information for objective function $f[x,\mu(x), u)$ and $h[x, \mu(x))$ are required for the controller design with the observable system states $x \in R^n$ and unknown nonlinear function $\mu(x)$. The inverse optimal design technique is used to develop the extremum seeking controller.

The RBF neural network was proposed in [21, 22] to approximate the nonlinear relation $\mu(x)$, i.e.

$$\mu\left[x(t)\right] = W^{*T} S\left[x(t)\right] + \mu_l(t) \quad (6)$$

where $\mu_l(t)$ is the approximation error, and the ideal weight W^* is obtained by

$$W^* := \arg\min_{W \in \Omega_w} \left\{ \sup \left| W^T S(x) - \mu(x) \right| \right\} \quad (7)$$

where $\Omega_w = \left\{ W \mid \|W\| \leq w_m \right\}$ and w_m is a positive constant, represents the upper bound of the weights, which is to be chosen at the design stage.

An adaptive learning technique using projection algorithm is used to online estimate the unknown parameters. A Lyapunov-based controller is designed to ensure the convergence of the system to an adjustable neighborhood of the optimum depends on the approximation error $\mu_l(t)$. The detailed formulation of the problem and the design procedure of the controller will be described in Section IV.

IV. AESC Based PV MPPT Control Design

The dynamics of the PV system in Fig. 4 can be described by two sets of differential equations based on different position of the switch [12]. The state equations with the switch *on* (State 1) can be given as

$$\frac{dV}{dt} = \frac{i(V)}{C} - \frac{i_L}{C} \quad (8)$$

$$\frac{di_L}{dt} = \frac{V}{L} - \frac{i_L}{R} \quad (9)$$

where $i(V)$ represents the complex nonlinear mapping between the output current and the terminal voltage of the PV array, i_L is the inductor current. If the switch is turned *off* (State 0), the state equations become

$$\frac{dV}{dt} = \frac{i(V)}{C} \quad (10)$$

$$\frac{di_L}{dt} = -\frac{i_L R}{L} \quad (11)$$

To obtain a unified system dynamics, Eqs. (8) through (11) are combined into a pair of state equations via a typical averaging method for PWM based switching circuits [23].

$$\frac{dV}{dt} = \frac{i(V)}{C} - \frac{i_L}{C} D \quad (12)$$

$$\frac{di_L}{dt} = -\frac{i_L R}{L} + \frac{V}{L} D \quad (13)$$

where duty ratio D is defined as the portion of State 1 within a period. To ensure a better approximation of the nonlinear relation $i(V)$ in the parameter updating process, the ranges of the PV output voltage V and the inductor current i_L are normalized, i.e. divided by 100 V and 10 A, respectively, which yields the following state and output equations

$$\frac{dx}{dt} = -\frac{R}{L} x + \frac{k_1}{L} su \quad (14)$$

$$\frac{ds}{dt} = \frac{k_2}{k_1 C} \mu(s) - \frac{1}{k_1 C} xu \quad (15)$$

$$y = k_1 k_2 \mu(s) s \quad (16)$$

where $x = i_L$, $s = V/k_1$ with $k_1 = 100$, $\mu(s) = i(V)/k_2$ with $k_2 = 10$, $y = P = iV$ is the power output of the PV array, and $u = D (0 \leq u \leq 1)$ is the control input to be designed by MPPT control.

At the steady state, the power output of the PV array can be expressed by

$$y_e = k_1 k_2 \mu(s_e) s_e \quad (17)$$

Following (6), the steady-state PV power output can be approximated by

$$y_e = k_1 k_2 W^{*T} S(s_e) s_e \quad (18)$$

with the first- and second-order derivatives being

$$\frac{\partial y_e}{\partial s_e} = k_1 k_2 W^{*T} \left[dS(s_e) s_e + S(s_e) \right] \quad (19)$$

$$\frac{\partial^2 y_e}{\partial s_e^2} = k_1 k_2 W^{*T} \left[d^2 S(s_e) s_e + 2dS(s_e) \right] \quad (20)$$

where $dS = \partial S/\partial s$ and $d^2S = \partial^2 S/\partial s^2$. The basis function vector $S(s)$ is given by

$$S(s) = \left[b_1(s) \quad b_2(s) \quad \ldots \quad b_l(s) \right] \quad (21)$$

$$b_i(s) = \exp\left[\frac{-(s - \varphi_i)^T (s - \varphi_i)}{\sigma_i^2} \right], \ i = 1, 2, \ldots, l \quad (22)$$

where φ_i and σ_i are the center and the width of the Gaussian function. For the function given by (21) and (22), we have

$$\frac{\partial S_i}{\partial s} = -2 \frac{(s - \varphi_i)}{\sigma_i^2} \exp\left[-\frac{(s - \varphi_i)^2}{\sigma_i^2} \right] \quad (23)$$

$$\frac{\partial^2 S_i}{\partial s^2} = \left(-2\frac{1}{\sigma^2} + 4\frac{(s - \varphi_i)^2}{\sigma^4} \right) \exp\left[-\frac{(s - \varphi_i)^2}{\sigma_i^2} \right] \quad (24)$$

The objective of the PV MPPT problem is then formatted as to develop a controller to maximizes the steady state power output y^* with a parameter estimation of the ideal weight W^*.

The design of the AESC controller mainly follows the procedure given in [22]. Substituting (6) into (14)-(16) yields

$$\dot{x} = -\frac{R}{L} x + \frac{k_1}{L} su \quad (25)$$

$$\dot{s} = \frac{k_2}{k_1 C} \left[W^{*T} S(s) + \mu_l(t) \right] - \frac{1}{k_1 C} xu \quad (26)$$

Let $\hat{W}$ denote the estimate of the true weights W^*, $\hat{s}$ and $\hat{x}$ denote the predictions of s and x, respectively. The predicted states equations can be given by

$$\dot{\hat{x}} = -\frac{R}{L}x + \frac{k_1}{L}su + k_x e_x + c_1(t)^T \dot{\hat{W}} \quad (27)$$

$$\dot{\hat{s}} = \frac{k_2}{k_1 C}\hat{W}^T S - \frac{1}{k_1 C}xu + k_s e_s + c_2(t)^T \dot{\hat{W}} \quad (28)$$

where k_x, k_s, $c_1(t)$ and $c_2(t)$ are parameters to be given. The state estimation errors $e_x = x - \hat{x}$ and $e_s = s - \hat{s}$ follow

$$\dot{e}_x = -k_x e_x - c_1(t)^T \dot{\hat{W}} \quad (29)$$

$$\dot{e}_s = \frac{k_2}{k_1 C}\tilde{W}^T S + \frac{k_2}{k_1 C}\mu_l(t) - k_s e_s - c_2(t)^T \dot{\hat{W}} \quad (30)$$

with $\tilde{W} = W^* - \hat{W}$. The optimum tracking error is defined as the difference between the estimated gradient and 0, i.e.

$$z = k_1 k_2 \hat{W}^T\left[dS(s)s + S(s)\right] \quad (31)$$

To make the parameters and states estimation converge towards their true values, a dither signal $d(t)$ is added, i.e.

$$z_s = \hat{W}^T\left[dS(s)s + S(s)\right] - d(t) \quad (32)$$

for which $k_1, k_2 > 0$ are removed for simplicity. The tracking error dynamics can be given as

$$\begin{aligned}\dot{z}_s &= \frac{d}{dt}\left\{\hat{W}^T\left[dS(s)s + S(s)\right] - d(t)\right\} \\ &= \dot{\hat{W}}^T\left[dS(s)s + S(s)\right] + \hat{W}^T\left[d^2S(s) + 2dS(s)\right]\dot{s} - \dot{d}(t)\end{aligned} \quad (33)$$

Let $\Gamma_1 = dS(s)s + S(s)$ and $\Gamma_2 = d^2S(s)s + 2dS(s)$, we have

$$\begin{aligned}\dot{z}_s &= \dot{\hat{W}}^T\Gamma_1 + \hat{W}^T\Gamma_2\dot{s} - \dot{d}(t) = \dot{\hat{W}}^T\Gamma_1 + \hat{W}^T\Gamma_2\left(\frac{k_2}{k_1 C}\hat{W}^T S(s)\right. \\ &\left. - \frac{1}{k_1 C}xu + \frac{k_2}{k_1 C}\tilde{W}^T S + \frac{k_2}{k_1 C}\mu_l\right) - \dot{d}(t)\end{aligned} \quad (34)$$

Define the variables

$$\eta_1 = e_x - c_1(t)^T \tilde{W} \quad (35)$$

$$\eta_2 = e_s - c_2(t)^T \tilde{W} \quad (36)$$

$$\eta_3 = z_s - c_3(t)^T \tilde{W} \quad (37)$$

Consider the Lyapunov function candidate

$$V = \frac{1}{2}\eta^T\eta = \frac{1}{2}\eta_1^2 + \frac{1}{2}\eta_2^2 + \frac{1}{2}\eta_3^2 \quad (38)$$

Take the time derivative of V, we have

$$\begin{aligned}\dot{V} &= \eta_1\dot{\eta}_1 + \eta_2\dot{\eta}_2 + \eta_3\dot{\eta}_3 \\ &= \eta_1\left(-k_x\eta_1 - k_x c_1(t)^T\tilde{W} - \dot{c}_1(t)^T\tilde{W}\right) \\ &+ \eta_2\left(\frac{k_2}{k_1 C}\tilde{W}^T S + \frac{k_2}{k_1 C}\mu_l - k_s\eta_2 - k_s c_2(t)^T\tilde{W} - \dot{c}_2(t)^T\tilde{W}\right) \\ &+ \eta_3\left(\dot{\hat{W}}^T\Gamma_1 + \hat{W}^T\Gamma_2\left(\frac{k_2}{k_1 C}\hat{W}^T S(s) - \frac{1}{k_1 C}xu + \frac{k_2}{k_1 C}\tilde{W}^T S\right.\right. \\ &\left.\left. + \frac{k_2}{k_1 C}\mu_l\right) - \dot{d}(t) - \dot{c}_3(t)^T\tilde{W} + c_3(t)^T\dot{\hat{W}}\right)\end{aligned} \quad (39)$$

By setting the dither signal as

$$\dot{d}(t) = c_3(t)^T\dot{\hat{W}}/(k_1 k_2) + \dot{\hat{W}}^T\Gamma_1 - k_d d(t) + \hat{W}^T\Gamma_2 a(t) \quad (40)$$

with k_d being a positive gain and external signal $a(t)$ to be assigned. Then the control law is

$$u = \frac{k_1 C}{x}\left[\frac{k_2}{k_1 C}\hat{W}^T S(s) - a(t) + \left(k_d / \hat{W}^T\Gamma_2\right)d(t) + \left(k_z / \hat{W}^T\Gamma_2\right)z_s\right] \quad (41)$$

We can reduce (39) to

$$\begin{aligned}\dot{V} &= \eta_1\left(-k_x\eta_1 - k_x c_1(t)^T\tilde{W} - \dot{c}_1(t)^T\tilde{W}\right) \\ &+ \eta_2\left(\frac{k_2}{k_1 C}\tilde{W}^T S + \frac{k_2}{k_1 C}\mu_l - k_s\eta_2 - k_s c_2(t)^T\tilde{W} - \dot{c}_2(t)^T\tilde{W}\right) \\ &+ \eta_3\left[-k_z\eta_3 - k_z c_3(t)^T\tilde{W} + \frac{\hat{W}^T\Gamma_2 k_2}{k_1 C}\left(\tilde{W}^T S + \mu_l\right) - \dot{c}_3(t)^T\tilde{W}\right]\end{aligned} \quad (42)$$

To cancel the terms with $\tilde{W}$, let

$$\dot{c}_1^T = -k_x c_1^T \quad (43)$$

$$\dot{c}_2^T = -k_s c_2^T + \frac{k_2}{k_1 C}S \quad (44)$$

$$\dot{c}_3^T = -k_z c_3^T + \frac{k_2}{k_1 C}\hat{W}^T\Gamma_2 S^T \quad (45)$$

Substituting (43)(44)(45) into (42) yields

$$\begin{aligned}\dot{V} &= -k_x\eta_1^2 - k_s\eta_2^2 + \frac{k_2}{k_1 C}\eta_2\mu_l - k_z\eta_3^2 + \frac{k_2}{k_1 C}\eta_3\hat{W}^T\Gamma_2\mu_l \\ &\le -k_x\eta_1^2 - k_s\eta_2^2 + \frac{k_2}{2k_1 k_3 C}\mu_l^2 + \frac{k_2 k_3}{2k_1 C}\eta_2^2 \\ &- k_z\eta_3^2 + \frac{k_2}{2k_1 C k_4}\mu_l^2 + \frac{k_4 k_2}{2k_1 C}\left(\hat{W}^T\Gamma_2\right)^2\eta_3^2\end{aligned} \quad (46)$$

where k_3 and k_4 are positive constants. To cancel the positive terms in (46), k_x, k_s and k_z can be designed as

$$k_x = k_{x0} \quad (47)$$

$$k_s = k_{s0} + \frac{k_2 k_3}{2k_1 C} \quad (48)$$

$$k_z = k_{z0} + \frac{k_4 k_2}{2k_1 C}\left(\hat{W}^T\Gamma_2\right)^2 \quad (49)$$

where k_{x0}, k_{s0} and k_{z0} are positive constants. We finally have

$$\dot{V} \le -\frac{k_m}{2}\eta^T\eta + \frac{k_2}{2k_1 Ck}\mu_l(t)^2 = -k_m V + \frac{k_2}{2k_1 Ck}\mu_l(t)^2 \quad (50)$$

with $k_m = 2\min\{k_{x0}, k_{s0}, k_{z0}\}$ and $k = 0.5\min\{k_3, k_4\}$. From [22], an explicit bound for $\|\eta\|$ can be obtained as

$$\|\eta\| \le \alpha_1 e^{\lambda_1(t - t_0)} + \sqrt{\frac{k_2}{2k_1 kC}}\sup_{t_0 \le \tau \le t}\left|\mu_l(\tau)\right| \quad (51)$$

with $\alpha_1 = \sqrt{V(t_0)}$ and $\lambda_1 = 1/(2k_m)$. Equation (51) assures the convergence of η to a small neighborhood of the origin. To show the convergence of the error signals e_x, e_s and z_s, we still need to ensure the convergence of the parameter estimation errors $\tilde{W}$ and also $c_1(t)$, $c_2(t)$, $c_3(t)$ are bounded.

The boundedness and the convergence of the parameter estimates $\hat{W}$ can be ensured by setting the following parameter update law and assigning the proper external signal $a(t)$ to provide the persistent excitation [22]:

$$\dot{\hat{W}} = \mathrm{Proj}\left(\Upsilon(t)e, \hat{W}\right) \quad (52)$$

where $\mathrm{Proj}\left(\Upsilon(t)e, \hat{W}\right)$ is the projection defined as

$$\mathrm{Proj}\left(\Upsilon(t)e,\hat{W}\right)$$
$$= \begin{cases} \gamma_w \Upsilon(t)^T e \begin{cases} \text{if } q(\hat{W}) \le w_m \\ \text{or if } q(\hat{W}) \ge w_m \text{ and } \gamma \hat{W}^T \Upsilon(t)^T e \le 0 \end{cases} \\ \gamma_w \left(I - \gamma^2 q(\hat{W}) \dfrac{\hat{W}\hat{W}^T}{\hat{W}^T\hat{W}} \right) \Upsilon(t)^T e \quad \text{otherwise} \end{cases} \tag{53}$$

where γ_w is a positive gain. The function $q(\hat{W})$ is given by

$$q(\hat{W}) = \left(M(\hat{W}) - w_m^2\right)/\epsilon^2 + w_m\epsilon \tag{54}$$

where w_m and ε are positive constants. $M(\hat{W})$ is given by

$$\begin{aligned} M(\hat{W}) &= \hat{W}^T\hat{W} + \ln\left(\left\|\mathrm{diag}\left[I\hat{W} - I(a-\delta)\right]\right\|^2\right) \\ &+ \ln\left(\left\|\mathrm{diag}\left[I(b-\delta) - I\hat{W}\right]\right\|^2\right) \end{aligned} \tag{55}$$

with a>0, b>0, δ>0. γ is defined with gradient grad[$q(\hat{W})$)

$$\begin{aligned} \gamma\hat{W}^T &= \mathrm{grad}\left[q(\hat{W})\right] = \hat{W}^T + \frac{1}{\left\|\mathrm{diag}\left[I\hat{W} - I(a-\delta)\right]\right\|}\hat{W}^T \\ &+ \frac{1}{\left\|\mathrm{diag}\left[I(b-\delta) - I\hat{W}\right]\right\|}\hat{W}^T \end{aligned} \tag{56}$$

To consider the boundedness of $c_1(t)$, $c_2(t)$, $c_3(t)$, let

$$\Upsilon(t)^T = \left[c_1(t) \quad c_2(t) \quad c_3(t)\right] \tag{57}$$

and from (43) through (45), we have

$$\dot{\Upsilon}(t) = -K(t)\Upsilon(t) + B(t) \tag{58}$$

with
$$K(t) = \begin{bmatrix} k_x & 0 & 0 \\ 0 & k_s & 0 \\ 0 & 0 & k_z \end{bmatrix} \tag{59}$$

$$B(t) = \left[0 \quad \frac{k_2}{k_1 C}S \quad \frac{k_2}{k_1 C}\hat{W}^T\Gamma_2 S^T\right]^T \tag{60}$$

Based on [22], to show $\Upsilon(t)$ is bounded, we need to show the elements of $B(t)$ are bounded functions of time with

$$\|B(t)\|^2 = \frac{k_2^2}{k_1^2C^2}S^TS + \frac{k_2^2}{k_1^2C^2}\left(\hat{W}^T\Gamma_2\right)^2 S^TS \tag{61}$$

Figures 2 and 3 show that s is bounded, and thus S,is bounded. Equations (23) and (24) also assure the boundedness of Γ_2. The above parameter update law leads to the boundedness of $\hat{W}$, implying the boundedness of $B(t)$ and then $\Upsilon(t)$.

V. Simulation Results

The AESC controller designed in last section was then simulated with the PV system described in Section II, on the platform of Simulink 7.3 SimPowerSystems with Matlab R2009a. The following initial parameters were set:

$$i_L(0) = 0.1A, V(0) = 0.1V, \hat{x}(0) = 0.1, \hat{s}(0) = 0.1$$

The design parameters in the adaptive controller (41) and the parameter update law (52) are chosen as: γ_w =100, k_d = 0.1, k_{z0} = 1, k_{x0} = 1000, k_{s0} = 1, k_3 = 1, k_4 = 0.1. To fully cover the range of [0,6], a 5-term RBF is selected with centers and widths of

$$\varphi_i = 0.6 + 4.8(i-1)/4 \text{ and } \sigma_i = 0.6, \quad i = 1,2,3,4,5$$

The initial weights are set as $\hat{W}_i(0) = 0.1$ for i = 1, 2, …, 5, and $a(t) = 10^{-4}\cdot\sum_{i=1}^{10}\omega_i\left[A_{1i}\sin(\omega_i t) + A_{2i}\cos(\omega_i t)\right]$, where A_{1i} and A_{2i}, i = 1,…,10, are randomly chosen from a unit normal distribution. The frequencies are chosen as

$$\omega_i = 100\cdot\left[1 + (i-1)10/9\right] \qquad i = 1,...,10$$

The initial values for $c_1(t)$, $c_2(t)$, $c_3(t)$ and $d(t)$ are given by

$$c_i(0)^T = [0 \quad 0 \quad 0 \quad 0 \quad 0],\ i = 1,2,3 \quad \text{and} \quad d(0) = 0$$

To evaluate the AESC performance, a dither ESC controller following [7] was simulated for the same example.

The performances of AESC and dither ESC with nominal conditions are compared in Fig. 5 with the same initial conditions as $i_L(0)$ = 22.1 A, $V(0)$ = 300 V. The theoretical maximum power at T = 25°C and G = 1000W/m^2 is 5884W. The steady-state MPPT result given by dither ESC is 5874W, and 5838W by the AESC. The AESC demonstrates a much quicker transient, with the 1% settling time of 0.035s compared to 0.4s for the dither ESC. The AESC has 0.78% steady-state error, as compared to 0.17% for the dither ESC.

Figure 6 shows a case of MPPT with a temperature change from 25°C (0 ~ 0.1s) down to 17°C (0.1 ~ 0.2s). The power outputs are 5876 W and 6061 W, respectively, with the dotted lines showing the theoretical optima, i.e. 5884W and 6082W, respectively. The bottom plot shows the control input u (i.e. D). Figure 7 shows the case with a step-down of the irradiance level from 1000W/m^2 (0 ~ 0.1s) to 500 W/m^2 (0.1 ~ 0.2s). The power outputs are 5876 W and 2501 W, with the theoretical optima (the dotted line) being 5884 W and 2576 W, respectively. Figure 8 shows the case of a simultaneous step change of both temperature (from 25 to 17°C) and irradiance. (from 1000 W/m^2 to 800 W/m^2). The power outputs are 5876 W and 4692 W, with the theoretical optima (the dot lines) being 5884W and 4695W, respectively.

VI. Conclusion

The AESC is applied to the PV MPPT problem, with the RBF approximating the unknown nonlinear I-V map. The duty ratio for the DC-DC converter is used to regulate the PV terminal voltage. Both the MPP and the unknown RBF parameters are learned by the adaptive update law. Simulation results show significant improvement in transient with the AESC over the dither ESC, with only slight increase of steady-state error. Similar improvement was also observed for abrupt ambient changes of temperature and irradiance.

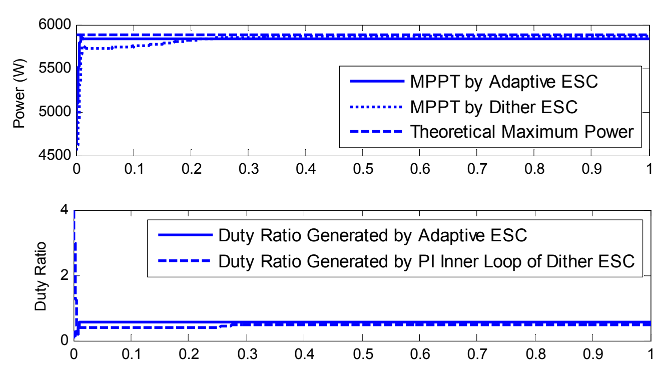

Fig. 5. Comparison of PV MPPT Results with AESC and Dither ESC.

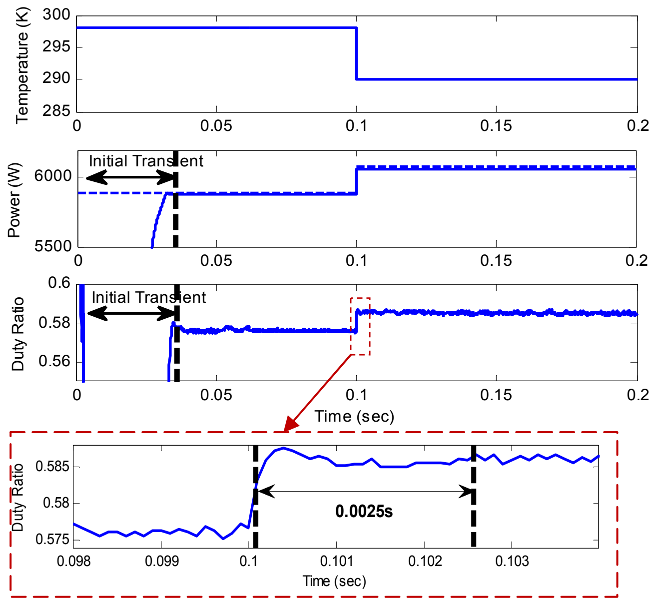

Fig. 6. AESC MPPT with a Step-down of Temperature.

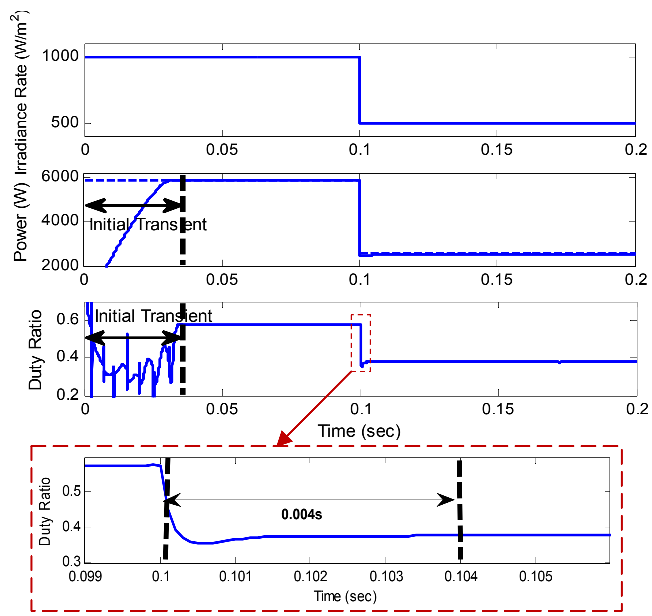

Fig. 7. MPPT with a Step Change of Irradiance Rate.

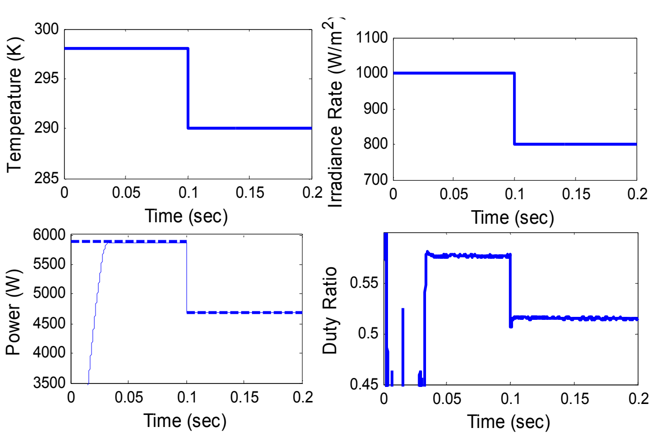

Fig. 8. MPPT with Step Change of Both Temperature and Irradiance Rate.

REFERENCES

[1] C. Martin. *Global Solar Energy May Reach 980 GW by 2020*. Available: http://www.seia.org/cs/news_detail?pressrelease.id=1132, 2010.

[2] H. P. Desai and H. K. Patel, "Maximum Power Point Algorithm in PV Generation: An Overview," in *Power Electronics and Drive Systems*, 2007, pp. 624-630.

[3] M. G. Villalva, *et al.*, "Comprehensive Approach to Modeling and simulation of Photovoltaic Arrays," *IEEE Trans on Power Electronics,* vol. 24, pp. 1198-1208, 2009.

[4] M. A. S. Masoum, *et al.*, "Theoretical and Experimental Analysis of Photovoltaic Systems with Voltage and current Based Maximum Power Point Tracking," *IEEE Trans on Energy Conversion,* vol. 17, pp. 514-522, 2002.

[5] M. Arutchelvi and S. Arul Daniel, "Voltage control of an autonomous hybrid generation scheme based on PV array and wind-driven induction generators," *Electric Power Components and Systems,* vol. 34, pp. 759-773, 2006.

[6] N. Femia, *et al.*, "Optimization of Perturb and Observe Maximum Power Point Tracking Method," *IEEE Trans Electronics,* **20**, 963-973, 2005.

[7] P. Lei, *et al.*, "Extremum Seeking Control Based Integration of MPPT and Degradation Detection for Photovoltaic Arrays," in *Proceedings of the 2010 American Control Conference,* pp. 3536-3541.

[8] R. Leyva, *et al.*, "MPPT of Photovoltaic Systems using Extremum-Seeking Control," *IEEE Trans Aerospace and Electronic Systems,* vol. 42, pp. 249-258, 2006.

[9] Y. C. Kuo, *et al.*, "Novel maximum-power-point tracking controller for photovoltaic energy conversion system," *IEEE Trans on Industrial Electronics,* vol. 48, pp. 594-601, 2001.

[10] E. Koutroulis, *et al.*, "Development of a microcontroller-based, photovoltaic maximum power point tracking control system," *IEEE Trans on Power Electronics,* vol. 16, pp. 46-54, 2001.

[11] T. Yoshida, *et al.*, "Simple control of photovoltaic generator systems with high-speed maximum power point tracking operation," *European Power Electronics and Drives Journal,* vol. 17, pp. 38-42, 2007.

[12] C.-C. Chu and C.-L. Chen, "Robust maximum power point tracking method for photovoltaic cells: A sliding mode control approach," *Solar Energy,* vol. 83, pp. 1370-1378, 2009.

[13] T. Noguchi, *et al.*, "Short-current pulse-based maximum power point tracking method for multiple photovoltaic and converter module system," *IEEE Trans on Industrial Electronics,* **49**, pp. 217-223, 2002.

[14] M. Krstic and H.-H. Wang, "Stability of extremum seeking feedback for general nonlinear dynamic systems," *Automatica,* vol. 36, pp. 595-601, 2000.

[15] M. Krstic, "Performance improvement and limitations in extremum seeking control," *Systems and Control Letters,* **39**, pp. 313-326, 2000.

[16] P. Lei, *et al.*, "Modeling and Global MPPT Control for Photovoltaic Array with Variable Shading," *IEEE Trans on Sustainable Energy,* vol. 2, pp. 348-358, July 2011 2011.

[17] V. Adetola and M. Guay, "Parameter convergence in adaptive extremum-seeking control," *Automatica,* vol. 43, pp. 105-110, 2007.

[18] M. Guay, *et al.*, "Adaptive extremum-seeking control of nonisothermal continuous stirred tank reactors," *Chemical Engineering Science,* vol. 60, pp. 3671-3681, 2005.

[19] D. DeHaan and M. Guay, "Extremum-seeking control of state-constrained nonlinear systems," *Automatica,* **41**, pp.1567-1574, 2005.

[20] M. Guay and T. Zhang, "Adaptive extremum seeking control of nonlinear dynamic systems with parametric uncertaintie," *Automatica,* vol. 39, pp. 1283-1293, 2003.

[21] R. M. Sanner and J. E. Siotine, "Gaussian networks for direct adaptive control," *IEEE Trans of Neural Networks,* vol. 3, pp. 837-863, 1992.

[22] M. Guay, *et al.*, "Adaptive extremum seeking control of continuous stirred tank bioreactors with unknown growth kinetics," *Automatica,* vol. 40, pp. 881-888, 2004.

[23] R. W. Erickson and D. Maksimovic, *Fundamentals of Power Electronics*: Kluwer Academic Publishers, 2001.